Asymmetric properties of the *Chlamydomonas reinhardtii* cytoskeleton direct rhodopsin photoreceptor localization

Telsa M. Mittelmeier,[1] Joseph S. Boyd,[1] Mary Rose Lamb,[2] and Carol L. Dieckmann[1]

[1]Department of Molecular and Cellular Biology, University of Arizona, Tucson, AZ 85721
[2]Department of Biology, University of Puget Sound, Tacoma, WA 98416

The eyespot of the unicellular green alga *Chlamydomonas reinhardtii* is a photoreceptive organelle required for phototaxis. Relative to the anterior flagella, the eyespot is asymmetrically positioned adjacent to the daughter four-membered rootlet (D4), a unique bundle of acetylated microtubules extending from the daughter basal body toward the posterior of the cell. Here, we detail the relationship between the rhodopsin eyespot photoreceptor Channelrhodopsin 1 (ChR1) and acetylated microtubules. In wild-type cells, ChR1 was observed in an equatorial patch adjacent to D4 near the end of the acetylated microtubules and along the D4 rootlet. In cells with cytoskeletal protein mutations, supernumerary ChR1 patches remained adjacent to acetylated microtubules. In *mlt1* (multieyed) mutant cells, supernumerary photoreceptor patches were not restricted to the D4 rootlet, and more anterior eyespots correlated with shorter acetylated microtubule rootlets. The data suggest a model in which photoreceptor localization is dependent on microtubule-based trafficking selective for the D4 rootlet, which is perturbed in *mlt1* mutant cells.

Introduction

Heterogeneity is an essential characteristic of living organisms that allows rapid adaptive responses to changes in the environment. One manifestation of heterogeneity within individual cells is their asymmetric organization; multisubunit complexes, organelles, and other subcellular structures are most often not distributed homogeneously, giving the cell an inherent polarity. In multicellular organisms, intracellular asymmetries are responsible for the innumerable cases in which cell division produces two daughter cells with different characteristics that, in turn, give rise to different cell types (Gönczy, 2008; Abrash and Bergmann, 2009; Sawa, 2010; St Johnston and Ahringer, 2010). Within a single cell, asymmetry enables polarized responses to environmental cues such as axon outgrowth in neurons (Quinn and Wadsworth, 2008) and the directional movement of motile cells (Vinogradova et al., 2009). One mechanism that generates or maintains asymmetry is the regulated trafficking of specific cellular components (Sann et al., 2009; Peters and Kropf, 2010; Poulain and Sobel, 2010). The microtubule cytoskeleton is a key player in intracellular transport and is itself inherently asymmetric as a result of age differences between the two centrosomes/basal bodies that nucleate the microtubules (Piel et al., 2000; Dutcher, 2003; Anderson and Stearns, 2009; Riparbelli et al., 2009; Wang et al., 2009; Yamashita, 2009) and the inherent directionality of the tubulin polymer (Li and Gundersen, 2008; Coquelle et al., 2009).

Chlamydomonas reinhardtii, a unicellular photosynthetic alga, has long served as an excellent model system with which to study the assembly, maintenance, and function of asymmetric cytoskeletal structures that allow the cell to respond to environmental cues (Holmes and Dutcher, 1989; Harris, 2001; Merchant et al., 2007). *C. reinhardtii* (Fig. 1 a) has two anterior flagella that beat in a breaststroke-like pattern, which propels the cell toward or away from light (phototaxis; Witman, 1993), Earth (gravitaxis; Yoshimura et al., 2003; Roberts, 2006), or a variety of biologically relevant molecules (chemotaxis; Sjoblad and Frederikse, 1981; Ermilova et al., 1993). Flagellar assembly is nucleated by two anterior basal bodies: the mother basal body, which was present throughout the previous cell cycle, and the

Correspondence to Carol L. Dieckmann: dieckman@email.arizona.edu

Abbreviations used in this paper: IFT, intraflagellar transport; TAP, Tris-acetate-phosphate.

The Rockefeller University Press $30.00
J. Cell Biol. Vol. 193 No. 4 741–753
www.jcb.org/cgi/doi/10.1083/jcb.201009131

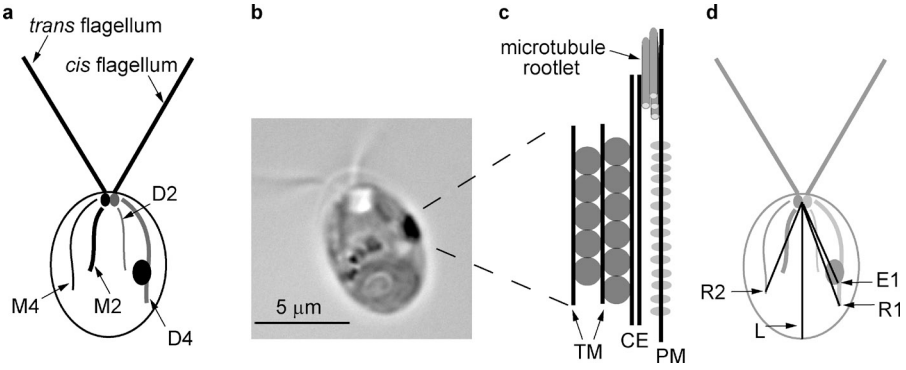

Figure 1. **The *C. reinhardtii* eyespot.** (a) A diagram illustrating asymmetric localization of the eyespot relative to the cytoskeleton. Two flagella and four microtubule rootlets extend from a pair of basal bodies at the anterior end of the cell; both the mother basal body (small black oval) and the daughter basal body (small gray oval) are associated with a four-membered rootlet (M4 or D4) and a two-membered rootlet (M2 or D2). The single eyespot (large oval) is associated with the four-membered daughter rootlet (D4), and the flagellum assembled from the daughter basal body is termed the cis-flagellum, whereas the trans-flagellum is assembled from the mother basal body. (b) A light micrograph of a wild-type *C. reinhardtii* cell showing the single large equatorial eyespot. (c) A diagram illustrating the components of the eyespot. Rhodopsin photoreceptors, including ChR1 (light gray ovals), in the plasma membrane (PM) directly apposed to the chloroplast envelopes (CE) and layers of carotenoid pigment granules (dark gray circles) subtended by thylakoid membrane (TM). The microtubules of the D4 rootlet are arranged in a three-over-one pattern. (d) A diagram of a *C. reinhardtii* cell (as in panel a) illustrating measurements discussed throughout the text and listed in Table I. L, cell length; R1, distance from the basal bodies to the tip of the most extensively acetylated rootlet; R2, distance from the basal bodies to the tip of the second most extensively acetylated rootlet; E1, distance from the basal bodies to the posterior edge of ChR1 photoreceptor–specific fluorescence.

daughter basal body, which was assembled during the previous cell cycle. The mother and daughter basal bodies differ in both their ultrastructure and their complement of associated proteins (Dutcher, 2003; Geimer and Melkonian, 2004), differences that presumably underlie the asymmetric beating patterns of the two flagella (Kamiya and Witman, 1984; Kamiya and Hasegawa, 1987; Takada and Kamiya, 1997; Rüffer and Nultsch, 1998) and the ability of the mother, but not the daughter, basal body to assemble a flagellum in the *uni* (uniflagellate) mutant background (Huang et al., 1982; Dutcher and Trabuco, 1998; Piasecki et al., 2008; Piasecki and Silflow, 2009). The basal bodies are thought to serve also as organizing centers for cytoplasmic microtubules, including the four acetylated microtubule rootlets that lie just beneath the cell membrane and extend from the basal bodies toward the posterior end of the cell (Ringo, 1967). Each basal body is associated with two rootlets, one that comprises two microtubules and one that comprises four microtubules in a three-over-one configuration (Moestrup, 1978; LeDizet and Piperno, 1986; Geimer and Melkonian, 2004; Harris, 2009). Observed from the flagellar pole, the four acetylated rootlets form a cruciate pattern that is offset from the plane of the flagella by 45°. The two four-membered rootlets, which are directly opposite one another, play a critical role in formation of the phycoplast at the cleavage plane during cytokinesis (Johnson and Porter, 1968; Holmes and Dutcher, 1989; Ehler and Dutcher, 1998).

After each cell division, the eyespot, the photoreceptive organelle required for phototaxis, is assembled de novo at an equatorial location opposite the cleavage furrow, adjacent to the newly formed daughter four-membered microtubule rootlet (D4; Fig. 1 a, D4; Holmes and Dutcher, 1989). The eyespot must be located at a specific position relative to the flagellar plane for photoreceptor activation and the resulting influx of Ca^{2+} to elicit movement in the correct direction (Foster and Smyth, 1980; Kamiya and Witman, 1984; Rüffer and Nultsch, 1991; Witman, 1993). In the light microscope (Fig. 1 b), the eyespot is visible as an orange-red oval ~1 μm in length located at the equator of the cell and is the most readily observable asymmetric feature of the otherwise green cells (Dieckmann, 2003; Kateriya et al., 2004; Kreimer, 2009). At the eyespot, rhodopsin photoreceptors in the plasma membrane lie directly over the closely apposed chloroplast envelope (Fig. 1 c; Melkonian and Robenek, 1980; Dieckmann, 2003; Kreimer, 2009). Two or three organized rows of carotenoid-filled lipid granules separated by thylakoid membrane are packed under the envelope and give the eyespot its orange color. The pigment granule layers reflect orthogonal light toward the photoreceptors and block light originating from other directions (Foster and Smyth, 1980). The placement and assembly of the eyespot is a unique example of asymmetric localization of a multicompartmental organelle in a well-characterized model system.

Several observations led to the long-standing hypothesis that asymmetric aspects of the *C. reinhardtii* cytoskeleton dictate eyespot placement (Holmes and Dutcher, 1989; Ehler et al., 1995; Kreimer, 2009). First, phototaxis requires specific localization of the eyespot relative to the flagella (Foster and Smyth, 1980). Second, observation of the eyespot pigment granule layers by bright field microscopy revealed that the eyespot was precisely positioned relative to other cytoskeletal structures throughout the cell cycle (Holmes and Dutcher, 1989). Third, EM and freeze-fracture studies showed a close association between the D4 rootlet and the eyespot (Gruber and Rosario, 1974; Melkonian and Robenek, 1980). However, the molecular mechanisms involved in eyespot assembly have remained uncharacterized. Are the photoreceptors associated with the D4 rootlet, as was previously observed for the pigment granule layers (Melkonian and Robenek, 1980; Holmes and Dutcher, 1989)? Is photoreceptor and/or pigment granule layer localization perturbed in mutants with supernumerary or disorganized cytoskeletal components? Does the *mlt1* mutation, which leads to the assembly of two or more stacks of pigment granule layers on opposite sides of the cell (Lamb et al., 1999), also affect localization of the photoreceptor? Does localization of the photoreceptor in the plasma membrane direct assembly of the pigment granule layers in the chloroplast, or vice versa? Alternatively, are eyespot components within each compartment localized independently?

To analyze the relationship between the Channelrhodopsin 1 (ChR1) photoreceptor and acetylated microtubules in both wild-type cells and in cells with mutations in cytoskeletal proteins,

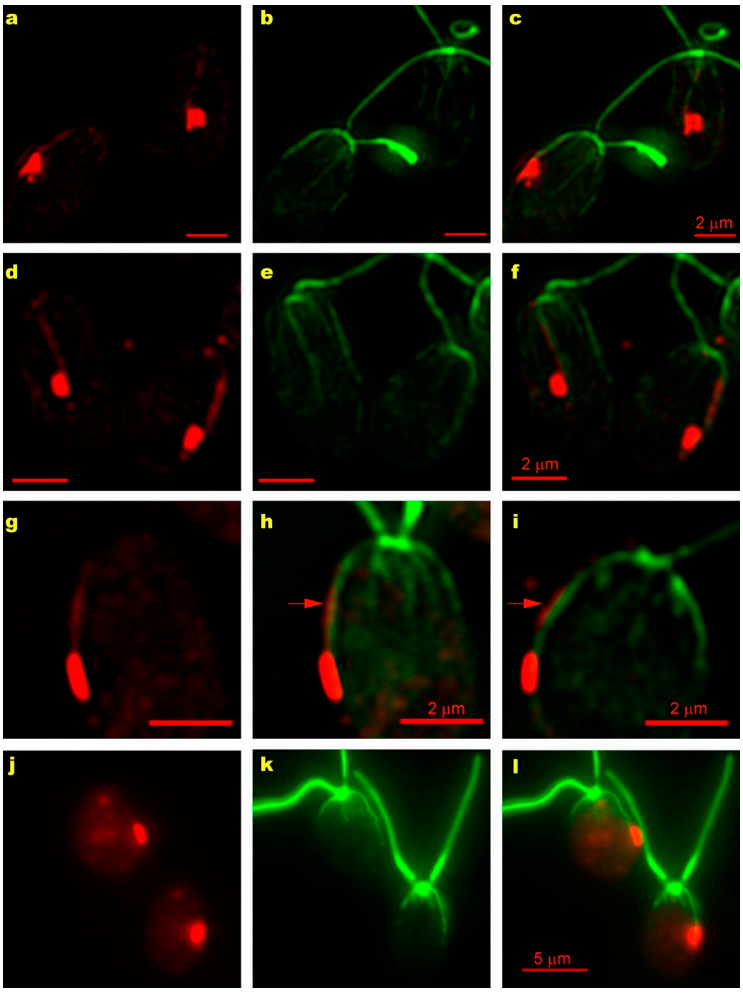

Figure 2. **The daughter microtubule rootlet is highly acetylated and is associated with the ChR1 photoreceptor.** (a–l) Fluorescence micrographs of wild-type cells (a–c, g, h, and j–l) or *uni1* cells (d–f and i), which only assemble the trans-flagellum, labeled with antiacetylated tubulin (green, b, e, and k) and anti-ChR1 (red, a, d, g, and j). Combined anti-ChR1 and antiacetylated tubulin fluorescence is shown in c, f, h, i, and l. A single patch of ChR1 was associated with the D4 rootlet in both wild-type and *uni1* cells. (g–i) Magnified images of the ChR1 stripe (red arrows) observed along the rootlet in some wild-type (g and h) and *uni1* (i) cells. (j–l) Combined fluorescence micrograph of wild-type cells labeled with anti-ChR1 (red) and antiacetylated tubulin (green) illustrates the association of the ChR1 patch with the most highly acetylated rootlet in wild-type cells in which R1/L = 0.68 ± 0.12 (n = 258), R1/R2 = 1.87 ± 0.58 (n = 131), and E1/L = 0.61 ± 0.06 (n = 128; Table I). The mean anterior–posterior length of the ChR1 patch was 0.94 ± 0.18 µm (n = 54). Bars: (a–i) 2 µm; (j–l) 5 µm.

we have used indirect immunofluorescence with antibodies directed against one of the major photoreceptors, ChR1 (Nagel et al., 2002; Suzuki et al., 2003; Govorunova et al., 2004; Berthold et al., 2008), and against acetylated tubulin, which specifically labels the flagella, basal bodies, and microtubule rootlets (Piperno and Fuller, 1985; LeDizet and Piperno, 1986). The data are consistent with the hypothesis that eyespot placement is dictated by the cytoskeleton, specifically by properties of the D4 rootlet. In wild-type cells, ChR1 was present in a single oval patch adjacent to the D4 daughter microtubule rootlet. In cells with mutations resulting in variable numbers of basal bodies and the associated rootlets, multiple ChR1 patches remained associated with acetylated microtubules. In *mlt1* mutant cells, multiple ChR1 patches that were associated with acetylated microtubules in both longitudinal halves of the cell were more anterior than in wild type, and the extent of acetylation along the D4 rootlet was diminished. However, the most posterior ChR1 patches were preferentially associated with daughter rootlets in *mlt1 uni1* double mutant cells, suggesting that the *mlt1* mutation perturbs the ChR1 localization process but does not lead to a complete loss of cellular asymmetry. ChR1 was also detected in spots at the anterior of the cell near the basal bodies and in a stripe along the D4 rootlet, suggestive of a model in which ChR1 is delivered from the Golgi to an anterior region of the plasma membrane, where it then diffuses or is transported along the D4 rootlet to its final equatorial location. In all strains, the pattern of pigment granule layer placement observed by light microscopy was similar to the pattern of ChR1 localization. Thus, we propose that asymmetric photoreceptor localization is a key step in eyespot assembly, promoting organization of the pigment granule and chloroplast membrane layers beneath the photoreceptor patch.

Results

The ChR1 eyespot photoreceptor is associated with the most extensively acetylated daughter rootlet

Previous microscopic studies described an association between the daughter four-membered acetylated microtubule rootlet (D4) and the pigment granule layers in the chloroplast portion of the eyespot (Fig. 1, a–c; Gruber and Rosario, 1974; Melkonian and Robenek, 1980; Holmes and Dutcher, 1989). Here, we have used immunofluorescence microscopy to explore the relationship between the D4 rootlet and the eyespot photoreceptor ChR1 in the plasma membrane. Methanol-fixed cells were double labeled with a monoclonal antiacetylated tubulin antibody (Piperno and Fuller, 1985; LeDizet and Piperno, 1986) and polyclonal serum directed against ChR1, an eyespot rhodopsin photoreceptor (Berthold et al., 2008). In each wild-type cell, a single large,

Table I. **Acetylated microtubule rootlet length and eyespot position in wild-type, *mlt1*, and *mlt1 uni1* cells**

Exp	Strain	*n*[a]	R1/L[b]	*n* (R2)[c]	R1/R2[d]	E1/L[e]	E[f]	E1 at D[g]	*n* (E2)[h]	E2/L	E2 at D[i]
							μm				
1	Wild type	54	0.66 ± 0.11	50	1.85 ± 0.62						
2	Wild type	51	0.66 ± 0.12	36	2.02 ± 0.53						
3	Wild type	53	0.58 ± 0.12	45	1.78 ± 0.56						
4	Wild type	100	0.75 ± 0.10								
1	*mlt1*	36	0.50 ± 0.12	33	1.33 ± 0.23						
2	*mlt1*	50	0.38 ± 0.14	47	1.42 ± 0.50						
3	*mlt1*	50	0.44 ± 0.12	50	1.55 ± 0.46						
4	*mlt1*	96	0.63 ± 0.15								
5	Wild type	22	0.69 ± 0.09			0.60 ± 0.06	1.02 ± 0.19				
6	Wild type	13	0.74 ± 0.10			0.65 ± 0.05	0.93 ± 0.14				
7	Wild type	19	0.66 ± 0.11			0.58 ± 0.05	0.84 ± 0.15				
8	Wild type	45	0.71 ± 0.07			0.61 ± 0.06					
9	Wild type	29	0.74 ± 0.10			0.64 ± 0.06					
10	Wild type	11				0.63 ± 0.06					
11	Wild type	16				0.63 ± 0.07					
12	Wild type	7				0.63 ± 0.05					
13	Wild type	35				0.67 ± 0.09					
15	*mlt1*	27				0.32 ± 0.13			16	0.23 ± 0.07	
16	*mlt1*	100				0.36 ± 0.10			42	0.27 ± 0.07	
17	*mlt1 uni1* uniflag. cells[j]	20				0.37 ± 0.15		17	11	0.19 ± 0.05	9
18	*mlt1 uni1* uniflag. cells	51				0.43 ± 0.15		41	23	0.24 ± 0.08	8
18	*uni1*	32				0.61 ± 0.10		31			

Exp, experiment number. Individual experiments were performed at separate times using unique cultures. Cells were analyzed by indirect immunofluorescence using antibodies specific for acetylated tubulin or the eyespot photoreceptor ChR1.

[a]Number of cells analyzed.

[b]Distance from the basal bodies to the end of the most highly acetylated rootlet (R1) relative to the anterior–posterior length of the cell (L), as diagrammed in Fig. 1 d. Each number presented is the mean of ratios obtained from individual cells and includes the SD within the experiment. R1/L values obtained from wild-type cells in experiments 1–4 (mean R1/L = 0.68 ± 0.12, *n* = 258) were significantly different than those obtained from *mlt1* cells (mean R1/L = 0.51 ± 0.17, *n* = 232) with P (0.05) = 1.6×10^{-28}.

[c]Number of cells in which the distance from the basal bodies to the second most highly acetylated rootlet (R2) was measured.

[d]R1/R2 values obtained from wild-type cells in experiments 1–3 (mean R1/R2 = 1.87 ± 0.58, *n* = 131) were significantly different than those obtained from *mlt1* cells (mean R1/R1 = 1.44 ± 0.44, *n* = 130) with P (0.05) = 1.5×10^{-10}.

[e]Distance from the basal bodies to the posterior end of the single ChR1 patch (wild-type and *uni1* cells) or the most posterior ChR1 patch (*mlt1* and *mlt1 uni1* cells; E1) relative to the anterior–posterior length of the cell (L), as diagrammed in Fig. 1 d. Each number presented is the mean of ratios obtained from individual cells and includes the SD within the experiment. E1/L values obtained from wild-type cells in experiments 5–13 (mean E1/L = 0.61 ± 0.06, *n* = 128) were significantly different than those obtained from *mlt1* cells in experiments 15 and 16 (mean E1/L = 0.35 ± 0.10, *n* = 126) with P (0.05) = 2.0×10^{-63} or from *mlt1 uni1* cells in experiments 17 and 18 (0.41 ± 0.15, *n* = 71) with P (0.05) = 1.4×10^{-17}. E1/L values obtained from *uni1* cells in experiment 18 (mean E1/L = 0.61 ± 0.1, *n* = 34) were not significantly different than wild-type values but were significantly different than those obtained from *mlt1 uni1* cells with P (0.05) = 1.1×10^{-17}.

[f]Anterior–posterior length of the ChR1 patch of the wild-type eyespot. The mean wild-type E = 0.94 ± 0.18 μm (*n* = 54, experiments 5–8).

[g]Number of *uni1* or *mlt1 uni1* cells in which the most posterior ChR1 patch was associated with a daughter rootlet.

[h]Number of *mlt1* or *mlt1 uni1* cells in which the distance from the basal bodies to the second most posterior ChR1 patch (E2) was measured.

[i]Number of *mlt1 uni1* cells in which the second most posterior ChR1 patch was associated with a daughter rootlet.

[j]Uniflagellate *mlt1 uni1* cells in which the association between ChR1 and the mother versus daughter halves of the cell was clear were chosen for analysis. Cells were from any one of six *mlt1 uni1* spores.

oval equatorial patch of ChR1 was observed (Fig. 2, a–c and j–l) that was 0.94 ± 0.18 μm in length (Table I). From the basal bodies, the distance to the posterior edge of the ChR1 patch relative to the length of the cell was 0.61 ± 0.06 (Fig. 1 d, E1/L; and Table I). The ChR1 patch was either adjacent to or overlapping with one of the microtubule rootlets, which are known to be highly acetylated relative to other cytoplasmic microtubules (LeDizet and Piperno, 1986). The ChR1 patch was to the right of the rootlet (counterclockwise if looking down the long axis of the cell from the flagellar pole; Figs. 2 c and 3 d) in 57% of the cells (*n* = 105), whereas in 43% of the cells, the ChR1 patch was to the left of the rootlet (clockwise if looking down the long axis of the cell from the flagellar pole; Fig. 3 a).

To verify that the ChR1-associated rootlet was a daughter rootlet, *uni1* mutant cells were labeled with the antiacetylated tubulin and anti-ChR1 antibodies (Fig. 2, d–f and i). The vast majority of *uni1* cells are uniflagellate because they fail to assemble the cis-flagellum from the daughter basal body (Huang et al., 1982). In 97% of *uni1* cells in which the identity of the daughter basal body and associated rootlet was clear (*n* = 172), the ChR1 patch was associated with a daughter rootlet. Based on previous studies, we assume that the ChR1-associated daughter rootlet was D4 (Gruber and Rosario, 1974; Holmes and Dutcher, 1989). Therefore, as observed for the pigment granules, the ChR1 photoreceptor is specifically and closely associated with the D4 rootlet.

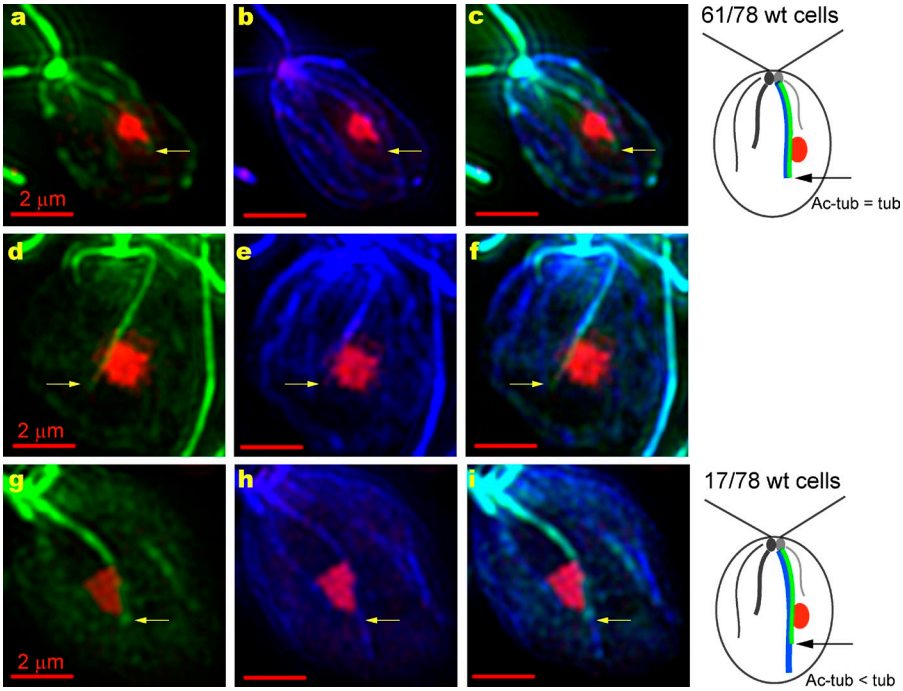

Figure 3. **Acetylation extends to the end of the D4 microtubule rootlet in most wild-type cells.** (a–i) Combined fluorescence micrographs of wild-type cells labeled with antiacetylated tubulin (green, a, d, and g), anti-ChR1 (red), and antitubulin (blue, b, e, and h) antibodies. The cells in a–c and g–i were labeled with antitubulin that was directly conjugated to Alexa Fluor 488, whereas isotype-specific secondary antibodies were used to detect the acetylated tubulin– and tubulin-specific fluorescence in the cell in d–f (see Materials and methods). (a–f) Two cells in which the acetylated tubulin–specific fluorescence extended to the posterior end of the tubulin-specific fluorescence (yellow arrows), as was the case for 61 of the 78 cells examined (top right diagram). The acetylated tubulin– and tubulin-specific fluorescence extended 0.75 ± 0.48 μm beyond the posterior edge of the ChR1 patch (n = 63). (g–i) A cell in which the tubulin-specific fluorescence extended beyond the posterior end of the acetylated tubulin–specific fluorescence (yellow arrows), as was the case for 17 of the 78 cells examined (bottom right diagram). For clarity, g–i are single images from the Z series (see Materials and methods).

In some wild-type and *uni1* cells, ChR1 was also observed in a stripe along the D4 rootlet (Fig. 2, c and f). The percentage of cells in which the ChR1 stripe along the D4 rootlet was observed varied between experiments from ~10% to >50%, perhaps because the presence of ChR1 on the rootlet is restricted to a specific portion of the cell cycle. The ChR1-specific stripe of fluorescence extended from the equatorial ChR1 patch toward the region of the basal bodies, following the path of the D4 rootlet exactly. In some edge-on micrographs (Fig. 2, g–i), the ChR1 stripe could be seen along the outer surface of the acetylated microtubules.

Upon closer examination of the pattern of antiacetylated tubulin fluorescence in wild-type and *uni1* cells, we noted that in most cells, one microtubule rootlet appeared consistently longer than the other distinguishable rootlets (Fig. 2, j–l). The mean distance from the basal bodies to the tip of the discernable antiacetylated tubulin fluorescence of this longest rootlet relative to the length of the cell was 0.68 ± 0.12 (Fig. 1 d, R1/L; and Table I). Thus, in most cells, this longest rootlet extended beyond the longitudinal midpoint (or equator) of the cell. On average, R1 was 1.87 ± 0.58–fold greater than the distance from the basal bodies to the tip of the discernable fluorescence along the second longest rootlet (Fig. 1 d, R1/R2; and Table I). In 81% of wild-type cells (n = 181) and 83% of *uni1* cells (n = 292), the ChR1 patch was associated with R1 (Fig. 2 l). The ChR1 patch was associated with one of two approximately equal length rootlets in 14% of wild-type and 12% of *uni1* cells and with a rootlet other than the longest in only 5% of either wild-type or *uni1* cells. Therefore, the more extensively acetylated rootlet is the D4 rootlet, and rootlet acetylation and/or length is an additional manifestation of asymmetry in the *C. reinhardtii* cell.

The D4 rootlet is acetylated along its entire length in the majority of wild-type cells

Acetylation of the D4 rootlet extended just beyond the posterior edge of the photoreceptor patch in the majority of wild-type cells (mean extension = 0.75 ± 0.48 μm, n = 63 cells). This raised the possibility that the extent of rootlet acetylation is regulated by an anterior–posterior marker, perhaps even the eyespot. Alternatively, the extent of acetylation might simply be determined by the length of the microtubules themselves. To distinguish between these possibilities, wild-type cells were triple labeled with anti-ChR1, antiacetylated tubulin, and antitubulin antibodies using two different protocols (see Materials and methods; Fig. 3). In 78% of cells in which the acetylated tubulin versus tubulin staining along the D4 rootlet was clear (n = 78 cells in three experiments), acetylation extended to the end of the D4 tubulin–specific fluorescence (two cells shown in Fig. 3, a–f). The microtubules extended beyond the acetylated tubulin–specific fluorescence in 22% of the cells (Fig. 3, g–i). The length of the nonacetylated extension was variable, averaging 0.94 ± 0.53 μm. These data indicate that the D4 rootlet is not necessarily acetylated along its entire length, suggesting that the extent of acetylation is regulated by additional factors. In these experiments, the D4 rootlet was distinguishable from other microtubules by its association with the ChR1 patch. However, we could not unequivocally distinguish the other rootlets from nonrootlet microtubules, so we could not compare the actual lengths of those rootlets with that of the D4 rootlet.

Eyespots are localized to both halves of the cell in *mlt1* mutants

mlt1 mutant cells were initially described as having two eyespots that were placed either on the same side of the cell or 180° from one another in approximately equal numbers (Lamb et al., 1999). Bright field micrographs of individual *mlt1* mutant cells are shown in Fig. 4 a. One eyespot was observed in only 19% (n = 188) of the *mlt1* cells examined, whereas 62% contained two eyespots and 19% contained three or more eyespots. In *C. reinhardtii*, a plane perpendicular to the plane of the flagella divides

the cis and trans halves of the cell containing cytoskeletal structures associated with the daughter or mother basal bodies, respectively (Holmes and Dutcher, 1989). Referencing this plane in *mlt1* cells with two eyespots (n = 117), both eyespots appeared to be in the same half of the cell in 59% of the cells and in different longitudinal halves in 41% of the cells.

To examine the localization of the ChR1 photoreceptor and its relationship to the microtubule rootlets in the *mlt1* mutant, cells were labeled with antiacetylated tubulin and anti-ChR1 only (Fig. 4 b) or in combination with antitubulin (Fig. 4 c). The majority of cells contained two or three larger patches of ChR1, and many additionally contained one to three small ChR1 patches. The ChR1 patches were more anterior in *mlt1* cells than in wild-type cells; the distance from the basal bodies to the posterior edge of the most posterior ChR1 patch relative to the length of the cell (E1/L) was 0.35 ± 0.10 (Table I), which differed significantly from E1/L in wild-type cells (0.61 ± 0.06; Table I). Aberrantly, ∼10% of the cells had large patches of ChR1 at the very anterior end of the cell near the basal bodies (Fig. 4, b and c, arrows), which were not included in the E1/L measurements. Although an association between these anterior ChR1 patches and a microtubule rootlet was unclear, the majority of ChR1 patches in *mlt1* cells were clearly adjacent to an acetylated rootlet. In 53% of cells with two rootlet-associated photoreceptor patches (n = 153), both patches were associated with a single rootlet, whereas in 47% of these cells, the ChR1 patches were associated with two rootlets. These data indicate that the *mlt1* mutation leads to the assembly of extraneous, nonequatorial ChR1 patches on rootlets other than D4.

In *mlt1* cells, antiacetylated tubulin–specific labeling of the ChR1-associated rootlets did not extend as far along the anterior–posterior axis of the cell as that of the D4 rootlet in wild-type cells. The mean distance from the basal bodies to the tip of the discernable fluorescence along the longest rootlet relative to the length of the cell (R1/L) was 0.51 ± 0.17 (Table I), which was significantly smaller than the R1/L measured in wild-type cells (0.68 ± 0.12; Table I). In *mlt1* cells, the ratio of the distance to the tip of the longest rootlet compared with that of the second longest rootlet (R1/R2) was 1.44 ± 0.44 (Table I), which was also significantly different than that measured for wild-type cells (1.87 ± 0.58; Table I). As R2 in *mlt1* cells was similar to wild type, the decrease in R1/R2 appeared to be a specific change in the length of acetylated R1 (the D4 rootlet in most wild-type cells).

The most posterior photoreceptor patch remains associated with a daughter rootlet in *mlt1 uni1* double mutant cells

Has asymmetric placement of the eyespot been completely lost in *mlt1* cells? Alternatively, in cells with multiple eyespots on the same side of the cell, do the eyespots remain associated with the daughter rootlet? To answer these questions, six *mlt1 uni1* double mutant strains were obtained from the spores of three nonparental ditype tetrads from a *mlt1* × *uni1* cross. All six double mutant strains had similar phenotypes, and data obtained from all of the strains were combined. Over half of the *mlt1 uni1* double mutant cells had more than one eyespot (Fig. 5, a–c).

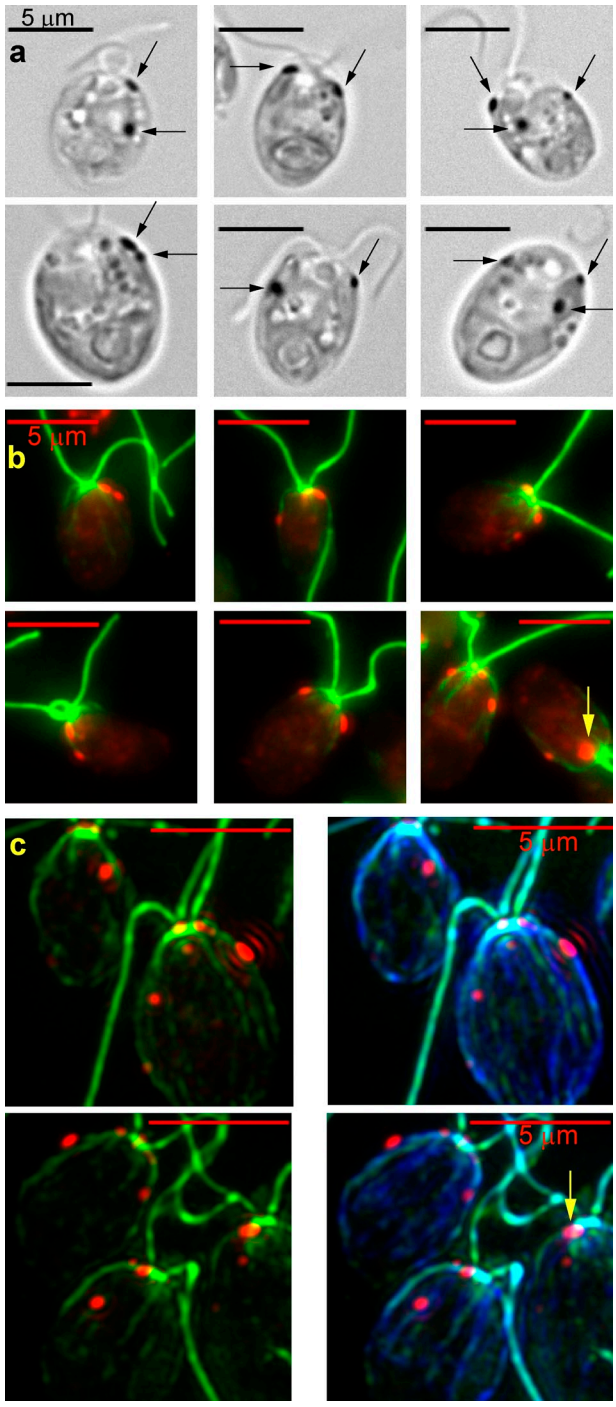

Figure 4. **The *mlt1* mutation leads to the assembly of eyespots in both the cis and trans halves of the cell.** (a) Light micrographs of *mlt1* mutant cells with two eyespots on the same side of the cell, eyespots in both the cis and trans halves of the cell, or three eyespots. The eyespots are indicated by arrows. (b) Combined fluorescence micrographs of *mlt1* mutant cells labeled with antiacetylated tubulin (green) and anti-ChR1 (red). The arrow points to a large patch of ChR1 at the anterior end of a cell. In *mlt1* cells, R1/L = 0.51 ± 0.17 (n = 232), R1/R2 = 1.44 ± 0.44 (n = 130), and E1/L = 0.35 ± 0.10 (n = 126; Table I). (c) Combined fluorescence micrographs of *mlt1* cells labeled with antiacetylated tubulin (green), anti-ChR1 (red), and antitubulin (blue) using isotype-specific secondaries for detection of anti-acetylated tubulin and antitubulin (see Materials and methods). The arrow points to a large patch of ChR1 at the anterior end of a cell.

54% of *mlt1 uni1* cells (n = 822) were uniflagellate, whereas 24% were biflagellate and 23% were aflagellate. As the single flagellum is templated by the mother basal body in *uni1* cells (Huang et al., 1982), we assumed that the same was true for the *mlt1 uni1* uniflagellate cells and proceeded to analyze the location of the ChR1 patches relative to the mother basal body and flagellum. The position of ChR1 patches along the anterior–posterior axis of these cells was also measured. In uniflagellate *mlt1 uni* cells (Fig. 5, d–g), the distance from the basal bodies to the most posterior ChR1 patch relative to the length of the cell (E1/L) was 0.41 ± 0.15 (Table I), which was significantly different than that of either wild-type or *uni1* cells (E1/L = 0.61 ± 0.10; Table I). In uniflagellate cells in which the association was clear, 82% of the most posterior patches of ChR1 were along rootlets associated with the daughter basal body (n = 71). In contrast, the second most posterior ChR1 patch (E2/L = 0.23 ± 0.08; Table I) was associated with the daughter basal body in only 50% of the cases examined (n = 34). These data indicate that the asymmetry of ChR1 localization is perturbed but is not completely lost in *mlt1* mutant cells.

Multiple eyespots are associated with acetylated tubulin in cells with mutations in cytoskeletal proteins

If localization of the eyespot is directed by asymmetric properties of the cytoskeleton, mutations that affect cytoskeletal organization would be expected to also affect eyespot placement. To test this hypothesis, eyespots in *asq2-1*, *vfl2*, and *bld2-1* mutant cells were analyzed by bright field and immunofluorescence microscopy. *ASQ2* encodes a conserved protein with three tubulin-binding cofactor C domains and is required for control of centriole number and positioning; *asq2-1* mutants have variable numbers of centrioles and flagella, and the daughter centrioles are often mislocalized to a more posterior position in the cell (Feldman et al., 2007; Feldman and Marshall, 2009). 34% of *asq2-1* cells (n = 92) had two or more eyespots visible by light microscopy (Fig. S1, a and b), and 37% (n = 264) had two or more patches of anti-ChR1 fluorescence (Fig. 6 a). In 83% of *asq2-1* cells with two ChR1 patches (n = 124), both patches were clearly associated with acetylated tubulin.

vfl2 cells have variable numbers of basal bodies and flagella as a result of defects in basal body segregation during cell division caused by a mutation in centrin (Wright et al., 1985, 1989; Taillon et al., 1992), a conserved calcium-binding protein present in several basal body substructures (Geimer and Melkonian, 2005). In agreement with previous observations of centrin-deficient cells (Koblenz et al., 2003), 19% of *vfl2* cells (n = 145) had two eyespots visible by light microscopy (Fig. S1, c and d), whereas 32% (n = 485) had two patches of ChR1 (Fig. 6 b). As for the *asq2* mutant, both patches of ChR1 were clearly associated with acetylated tubulin in 84% of *vfl2* mutant cells with two ChR1 patches (n = 121).

The *BLD2* gene encodes ε-tubulin, a conserved component of basal bodies (Dutcher et al., 2002). *bld2-1* cells lack basal bodies, are aflagellate, and have disorganized microtubule rootlets (Goodenough and StClair, 1975; Ehler et al., 1995). 75% of *bld2-1* cells (n = 126) had a single eyespot visible with the light microscope (Fig. S1, e and f), 11% had no eyespot, and 14% had two eyespots. By immunofluorescence, at least 45% of *bld2-1* cells (n = 179) had a single patch of ChR1, 5% had two patches, and up to 50% did not have clearly discernable ChR1 patches. The discrepancy between the number of *bld2* cells that contained pigment granule patches and the number that contained ChR1 patches can be explained by the observation that the pigment granule patches were extremely small in some *bld2* cells (Fig. S1 f). Although these pigment granule patches remained identifiable by their red color, the very small spots of ChR1 associated with these granules were not categorized as ChR1 patches in the analysis of fluorescence micrographs. In all cases (n = 80), ChR1 patches were associated with rootlets (Fig. 6 c). Though the specific identity of the supernumerary ChR1-associated rootlets in the mutant cells remains unknown, the consistent association between ChR1 patches and acetylated microtubule rootlets is supportive of the hypothesis that the cytoskeleton, specifically the microtubule rootlet structure, directs ChR1 localization.

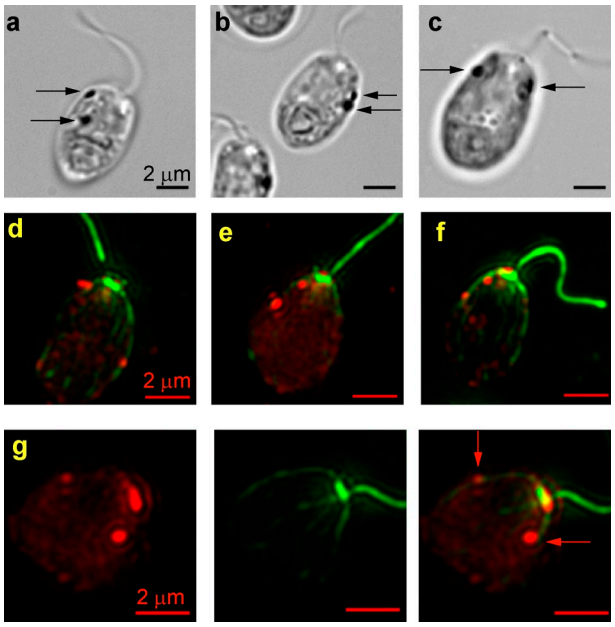

Figure 5. **The most posterior photoreceptor patch remains associated with a daughter rootlet in *mlt1 uni1* double mutant cells.** (a–c) Bright field micrographs of *mlt1 uni1* cells that contained two eyespots (arrows). (d–f) Combined fluorescence micrographs of individual *mlt1 uni1* uniflagellate cells labeled with antiacetylated tubulin (green) and anti-ChR1 (red). The most posterior patch of ChR1-specific fluorescence was associated with a daughter acetylated rootlet in 82% of *mlt1 uni1* uniflagellate cells (n = 71), whereas the second most posterior ChR1 patch was associated with the daughter rootlet in 50% of the cells examined (n = 34). (g) A uniflagellate *mlt1 uni1* cell labeled with anti-ChR1 (red) and antiacetylated tubulin (green) that contained both anterior ChR1 and two ChR1 patches (arrows). The most posterior ChR1 patch was associated with a daughter microtubule rootlet.

Small ChR1 spots are located near the basal bodies

Microtubule rootlets could direct ChR1 localization by specific trafficking of the photoreceptor from points of delivery to the plasma membrane, posteriorly along the daughter four-membered rootlet, to the appropriate equatorial location. Microtubules are

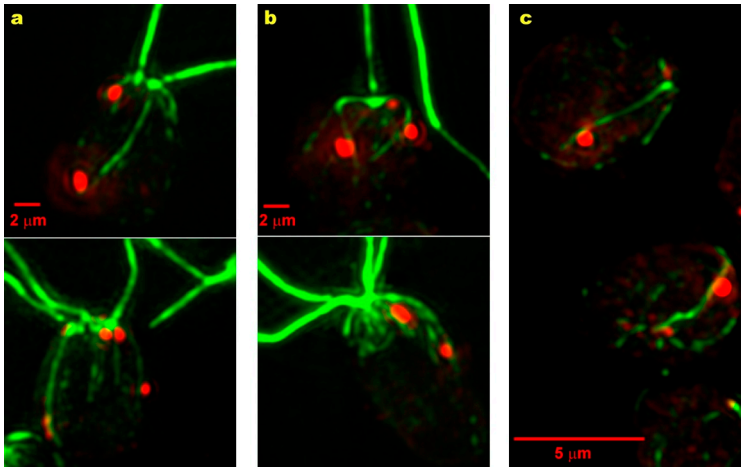

Figure 6. **ChR1 is associated with acetylated microtubules in cells with mutations in cytoskeletal proteins.** (a–c) Combined fluorescence micrographs of *asq2-1* cells (a), *vfl2* cells (b), or *bld2-1* (c) cells labeled with antiacetylated tubulin (green) and anti-ChR1 (red).

known to serve as tracks for intraflagellar transport (IFT), the movement of flagellar components into and out of the flagella. In *C. reinhardtii*, the isolation of mutants that are aflagellate and unable to swim has led to the identification and characterization of a large number of proteins involved in IFT. To determine whether proteins required for IFT are also required for photoreceptor localization, the following mutants, in which either anterograde or retrograde transport is defective, were analyzed by bright field and immunofluorescence microscopy: *fla3-1* (*ts* mutation in kinesin-associated protein of heterotrimeric kinesin-2; Mueller et al., 2005), *fla8-1* (*ts* mutation in a kinesin-2 motor subunit; Miller et al., 2005), *fla10-1* (*ts* mutation in a kinesin-2 motor subunit; Walther et al., 1994; Vashishtha et al., 1996; Iomini et al., 2001; Miller et al., 2005), *fla15-1* (*ts* mutation in IFT44; Piperno et al., 1998; Iomini et al., 2001, 2009), *fla17* (*ts* mutation in IFT39; Piperno et al., 1998; Iomini et al., 2001, 2009), *bld1* (IFT52; Brazelton et al., 2001; Deane et al., 2001), and *stf1-1* (cytoplasmic dynein heavy chain 1b; Pazour et al., 1999; Porter et al., 1999). Single eyespots at an approximately equatorial location were observed by bright field microscopy in all mutant cells (unpublished data). Immunofluorescence microscopy also confirmed the presence of a single equatorial patch of ChR1 in cells from all mutant cultures; representative micrographs of *fla8-1*, *bld1*, and *fla15-1* cells are shown in Fig. 7 (a, b, and d). Therefore, the IFT proteins represented by the mutant strains analyzed, including the anterograde and retrograde motors kinesin-2 and cytoplasmic dynein, respectively, are not required for ChR1 localization.

Although localization of the equatorial photoreceptor patch appeared normal in the IFT mutants, relatively small spots of anti-ChR1 fluorescence near the basal bodies were prominent in many of the aflagellate cells (Fig. 7, arrows). These spots appeared more peripheral than previously observed staining with antibodies specific for components of the basal body (Dutcher et al., 2002; Piasecki and Silflow, 2009) or proteins involved in IFT (Mueller et al., 2005) and often appeared to be like handlebars flanking the basal bodies. Upon closer examination, very small anterior ChR1 spots were also present in some wild-type cells (Fig. 7, c and e). The level of ChR1-specific fluorescence in anterior ChR1 spots in aflagellate cells was compared with that in wild-type cells by measuring the mean pixel density of the brightest anterior spot in wild-type and *fla8-1* or *fla15-1* cells grown at the restrictive temperature and mixed before staining. Measurement of mean pixel intensities (see Materials and methods) indicated that a larger proportion of aflagellate cells had significantly higher levels of anterior ChR1-specific fluorescence. The distribution of mean pixel densities in wild-type cells compared with those of the aflagellate mutant cells is shown in Fig. 7 e. Though the IFT mutations examined here did not grossly affect ChR1 localization, an unidentified localization mechanism may be perturbed in cells that are unable to assemble flagella, resulting in the accumulation of anterior ChR1.

Discussion

The *C. reinhardtii* photoreceptive eyespot is located at the equator of the cell, adjacent to the four-membered acetylated microtubule rootlet associated with the daughter basal body (D4). The asymmetric placement of the eyespot is necessary for the cell to swim toward or away from a light source. The eyespot photoreceptor ChR1 is a rhodopsin family light-activated cation channel localized to the plasma membrane directly above the eyespot pigment granule layers in the chloroplast (Melkonian and Robenek, 1980; Nagel et al., 2002; Berthold et al., 2008). Here, we have used immunofluorescence microscopy to analyze the relationship between the eyespot photoreceptor ChR1 and the four acetylated microtubule rootlets that extend from the basal bodies at the anterior end of the cell. Our data are consistent with the long-standing hypothesis that the asymmetric properties of the *C. reinhardtii* cytoskeleton direct eyespot placement (Moestrup, 1978; Holmes and Dutcher, 1989; Ehler et al., 1995; Ehler and Dutcher, 1998). In addition, the data show that the product of the *MLT1* gene restricts ChR1 localization to the D4 rootlet and promotes equatorial assembly of the eyespot, perhaps via an effect on microtubule rootlet acetylation.

Both in wild-type cells and in *uni1* cells, which assemble a single flagellum from the mother basal body (Huang et al., 1982), ChR1 was present in a single patch adjacent to the D4 rootlet. What directs asymmetric localization of ChR1 to the D4 rootlet? Photoreceptor localization is most likely independent of the organized assembly of pigment granule layers in the chloroplast. The correct asymmetric localization of an eyespot photoreceptor

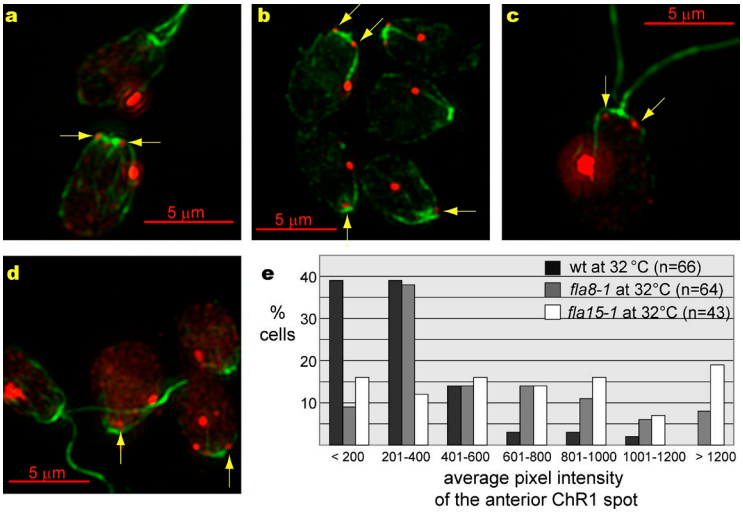

Figure 7. **Spots of ChR1 are located near the basal bodies in both wild-type and aflagellate mutant cells.** (a–d) Combined fluorescence micrographs of cells labeled with antiacetylated tubulin (green) and anti-ChR1 (red). The arrows point to anterior spots of ChR1. (a) Wild-type (cell with flagella) and *fla8-1* (aflagellate) cells were grown at 32°C and mixed before labeling. (b) *bld1* cells. (c) Wild-type cell. (d) Wild-type and *fla15-1* cells were grown at 32°C and mixed before labeling. (e) Distribution of the mean pixel intensity of the anterior ChR1 spot. The y axis indicates the percentage of wild-type (wt) or aflagellate *fla8-1* or *fla15-1* mutant cells (grown at 32°C) analyzed. The x axis indicates binned mean pixel intensities of fluorescence representing the brightest anterior spot of ChR1. X axis values were obtained from micrographs that contained images of both wild-type and aflagellate mutant cells grown at 32°C and mixed before methanol fixation. The wild-type values differed significantly from the values obtained from either *fla8-1* (P (0.05) = 2.35×10^{-7}) or *fla15-1* (P (0.05) = 3.78×10^{-5}) mutant cells.

was hypothesized to be responsible for the restoration of photoresponses by all-trans retinal in a carotenoid-deficient strain that did not form observable pigment granule layers (Lawson and Satir, 1994). Similarly, ChR1 was observed in eyespotlike patches on one side of the cell in both *eye2* and *eye3* (eyeless) mutant cells (Boyd et al., 2011) that are devoid of observable pigment granule layers (Lamb et al., 1999; Roberts et al., 2001) and in *min1* (minieyed) mutant cells under conditions in which the pigment granules are disorganized and no longer apposed to the plasma membrane (Lamb et al., 1999; Mittelmeier et al., 2008). However, the data do not rule out the possibility that other plastid components are required for photoreceptor localization. To determine whether the presence of aberrant rootlets (as opposed to the absence of pigment granule layers) led to altered localization of ChR1, we examined the eyespot phenotype of several mutant strains with variable numbers of basal bodies and disorganized cytoskeletons caused by mutations in cytoskeletal proteins. In *bld2-1* cells, in which a mutation in ε-tubulin disrupts basal body assembly and microtubule rootlet organization (Goodenough and StClair, 1975; Ehler et al., 1995), ChR1 remained associated with acetylated microtubules. In *asq2-1* or *vfl2* cells, which contain mutations that disrupt basal body assembly and/or segregation (Taillon et al., 1992; Feldman et al., 2007), ChR1 remained associated with acetylated microtubule rootlets in the 20–30% of cells with two ChR1 patches. The observation that cells with mutations in cytoskeletal components have supernumerary ChR1 patches associated with acetylated microtubules identifies photoreceptor localization as a downstream effect of cytoskeletal organization.

In both wild-type cells and in the cytoskeletal protein mutant cells analyzed, not all acetylated microtubules were associated with patches of ChR1. These data underscore the specificity of the eyespot photoreceptor for only a subset of acetylated microtubules, presumably those that are analogous to the D4 rootlet in wild-type cells. The *MLT1* gene product promotes this specificity for the D4 rootlet. In nearly half of *mlt1* mutant cells with two or more ChR1 patches, a photoreceptor patch was associated with a rootlet other than D4. The analysis of *mlt uni1* double mutant cells showed that the most posterior photoreceptor patch was associated with a daughter rootlet in 82% of the cells examined, but the second most posterior patch was distributed equally between the mother and daughter halves of the cell. We have formulated two hypotheses to explain these observations: one is based on asymmetric localization of MLT1, and the other is based on the timing of *MLT1* expression and/or function. Mother basal bodies differ from their daughters in having fewer "tiers" present in the distal cartwheel structure (Geimer and Melkonian, 2004) and in their competence to assemble a flagellum in the *uni* mutant background (Huang et al., 1982; Dutcher and Trabuco, 1998; Piasecki et al., 2008; Piasecki and Silflow, 2009). The association of the *MLT1* gene product with either the mother or the daughter basal body and/or rootlets could block (mother) or promote (daughter) ChR1 localization; however, this does not explain the correct placement of the most posterior eyespots in *mlt1 uni1* cells. The *uni* phenotypes have prompted the hypothesis that after cell division, daughter basal bodies undergo a maturation process before flagellar assembly (Dutcher, 2003; Harris, 2009). Asymmetric localization of MLT1 may not be necessary for assuring the asymmetric localization of ChR1 until after the daughter structures have matured. Alternatively, the eyespot may be assembled initially at the correct location with cues from mother–daughter cytoskeletal differences that are independent of the *MLT1* gene product. Subsequent to daughter basal body maturation, *MLT1* expression and/or function would block all new eyespot formation in the cell.

How is ChR1 localized to a specific equatorial patch of plasma membrane adjacent to the D4 rootlet? In addition to the photoreceptor patch at the eyespot, ChR1 was observed in smaller spots that were peripheral to the basal bodies and along the D4 rootlet in close association with the acetylated microtubules. In edge-on micrographs in which the ChR1-specific fluorescence was resolved from that of acetylated tubulin, the stripe was observed along the outer edge of the microtubules. The observed pattern of ChR1 localization could result from random diffusion of the photoreceptor within the plasma membrane until binding sites associated with the D4 microtubules are encountered. Alternatively, ChR1 may be targeted from the

trans-Golgi to regions near the base of the flagella, as has been reported for components of the flagella (Vashishtha et al., 1996; Pazour et al., 1999; Deane et al., 2001; Qin et al., 2007; Baldari and Rosenbaum, 2010), and may associate, directly or indirectly, with the anterior portion of the D4 rootlet. ChR1 might then diffuse along the rootlet to its final equatorial location or might associate with a microtubule-based motor that moves toward the plus end of the D4 microtubules. Mutations in components of the *C. reinhardtii* heterotrimeric kinesin-2 required for anterograde IFT did not disrupt ChR1 localization to equatorial patches adjacent to D4. However, the *C. reinhardtii* genome encodes at least 20 other proteins with predicted kinesin motor domains (Richardson et al., 2006), one or more of which might participate in ChR1 transport along the D4 rootlet.

Whatever the mechanism of ChR1 transport, the *MLT1* gene product promotes the equatorial placement of the eyespot. ChR1 patches were more anterior in *mlt1* cells than in wild-type cells, and up to 10% of *mlt1* cells accumulated ChR1 at the anterior end of the cell near the basal bodies. Acetylated D4 length was also reduced in *mlt1* cells. Perhaps, as has been observed in other systems (Hammond et al., 2008), microtubule acetylation and/or other posttranslational modifications affected by the *mlt1* mutation promote ChR1 trafficking along the D4 rootlet. The observation that acetylation did not extend to the end of the D4 microtubules in 22% of cells examined implies that rootlet acetylation is regulated. An effect of *MLT1* on the regulation of D4 acetylation at a specific time during the cell cycle could explain the loss of both specificity for and posterior movement along the D4 rootlet in *mlt1* mutant cells. *MLT1* might also affect ChR1 localization via effects on the actin fibers associated with the microtubule rootlets (Ehler et al., 1995; Ehler and Dutcher, 1998) or on the striated microtubule-associated fibers that form an asymmetric cross at the anterior ends of the four rootlets (Lechtreck and Melkonian, 1991; Lechtreck and Silflow, 1997). Visualization of ChR1, acetylated microtubules, and other proteins potentially involved in ChR1 localization throughout the cell cycle in both wild-type and mutant cells should help define the mechanism of photoreceptor localization.

Is localization of the photoreceptor or of associated plasma membrane and cytoplasmic components of the eyespot sufficient for localization of the eyespot pigment granule layers in the chloroplast? In *asq2-1*, *vfl2*, *mlt1*, and *mlt1 uni1* cells, the pattern of pigment granule layer localization observed by bright field microscopy was similar to localization of the photoreceptor patches observed by immunofluorescence, and, in *mlt1* cells, the presence of multiple assemblies of organized pigment granules was verified by EM (Lamb et al., 1999). This correlation is consistent with the hypothesis that an aberrantly localized photoreceptor promotes the assembly of the associated pigment granules. Alternatively, each mutation might independently affect placement of both the photoreceptor and the pigment granule layers by altering a common component of both localization pathways, such as the D4 rootlet. A model in which asymmetric localization of ChR1 via cytoskeletal-directed trafficking is required for assembly of the pigment granule layers in the chloroplast can be tested by the construction and phenotypic analysis of cells with mutations in ChR1 and/or the photoreceptor localization pathway. A detailed description of the mechanism by which the coordinated asymmetric placement of eyespot components in both the plasma membrane and the chloroplast is achieved will add to our understanding of asymmetry in all eukaryotic cells.

Materials and methods

Strains and media

C. reinhardtii wild-type strain 137c *mt*$^+$ (stock CC-125; *Chlamydomonas* Center, Duke University) was used throughout this study. The *mlt1* mutant strain 12–10 (137c *mlt1 mt*$^+$) was obtained by UV mutagenesis of strain 137c *mt*$^+$ followed by screening for mutants that were unable to phototax (Lamb et al., 1999). Six *mlt1 uni1* double mutant strains were obtained from a cross of strain 12–10 *mt*$^-$ (*mlt1 mt*) to strain *uni1-1 mt*$^+$ (CC-1926). From this cross, 51 tetrads yielded 17 parental ditypes, 3 nonparental ditypes, and 31 tetratypes. The six double mutant spores from the three nonparental ditype tetrads were used for further analysis. *asq2-1* (CC-4301) was a gift from W. Marshall (University of California, San Francisco, San Francisco, CA). All other strains were obtained from E. Harris (Duke University, Durham, NC) and M. Laudon (University of Minnesota, St. Paul, MN) at the *Chlamydomonas* Resource Center and are cataloged as follows: *vfl2* (CC-2530), *bld2-1* (CC-478), *fla3-1* (CC-4283), *fla8-1* (CC-1396), *fla10-1* (CC-1919), *fla15-1* (CC3861), *fla17-1* (CC-3863), *bld1* (CC-477), and *stf1-1* (CC-3915).

C. reinhardtii cultures were maintained on solid Tris-acetate-phosphate (TAP) medium or TAP + 0.2 mg/ml arginine (Harris, 2009). For phototaxis assays or microscopy, cells from 2–3-d solid TAP medium cultures were used to inoculate liquid-modified Sager and Granick medium I with Hutner's trace elements (M medium). The liquid cultures were grown photoautotrophically for 16–20 h at either 25°C or at 32°C (restrictive temperature for temperature-sensitive mutant strains). All cultures were grown under continuous light.

Light microscopy

10 µl of an overnight liquid culture was spotted onto a microscope slide and coverslipped. The cells were viewed with a microscope (DMRXA; Leica) using a PL APO 100×, 1.4 numerical aperture oil immersion objective (Leica) with a 1.6× optivar (1 pixel = 0.039 µm) and bright field optics. After 5–10 min on the slide, the flattened, less motile cells were photographed. Images were captured with a camera (Retiga EX-cooled CCD; QImaging) driven by MetaMorph v.6.1.2 software (Universal Imaging).

Immunofluorescence labeling

Inocula from fresh cultures on solid medium were transferred to 2 ml of liquid M medium and grown overnight at 25 or 32°C (restrictive temperature for strains *fla3-1*, *fla8-1*, *fla10-1*, *fla15-1*, and *fla17-1*) under continuous light. Cells were harvested from 0.5 ml of culture at 2,700 *g* for 10 min, resuspended in *C. reinhardtii* autolysin prepared from strains 4A$^+$ and 1B$^-$ (a gift from P. Hamel, Ohio State University, Columbus, OH), and incubated for 1 h at room temperature. The cells were harvested, resuspended in PBS, spotted onto 10-well poly-L-lysine–coated slides, allowed to settle for 10 min at room temperature, and then dipped into −20°C methanol for 20–30 s. After a brief drying period, the cells were incubated in block buffer (1× PBS and 1% BSA) for 1 h at room temperature and then overnight at 4°C with block buffer containing 1:50 polyclonal anti-ChR1 (a gift from P. Hegemann, Humboldt-Universität zu Berlin, Berlin, Germany; Berthold et al., 2008) plus 1:10 monoclonal antiacetylated tubulin, clone 6-11B (Sigma-Aldrich; Piperno and Fuller, 1985). The cells were washed four times for 10 min in wash buffer (block buffer plus 0.1% Tween-20) and incubated in 1:1,000 donkey anti–rabbit Alexa Fluor 594 plus 1:1,000 goat anti–mouse Alexa Fluor 488 (both from Invitrogen) for 2 h at room temperature. After rinsing with wash buffer followed by PBS, cells were coverslipped using either a hard set mounting medium (VectaShield; Vector Laboratories) or a mounting medium (Mowiol; EMD) prepared as follows: 2.4 g MOWIOL 4–88 Reagent (EMD) was added to 6 g glycerol, stirred, combined with 6 ml of water, stirred at room temperature for 2 h, combined with 12 ml of 0.2-M Tris, pH 8.5, and heated to 50°C for 10 min. The solution was clarified by centrifugation at 5,000 *g* for 15 min and stored in airtight tubes at −20°C. For experiments that included antibodies directed against tubulin, the cells were cultured and treated as described in this section, except for the −20°C MeOH treatment, which was extended to 20 min. Microtubules were labeled with either 1:200 antitubulin (clone DM 1A)

directly conjugated to the Alexa Fluor 488 (eBioscience; Fig. 3, a and c) or with 1:50 unconjugated antitubulin (clone DM 1A; Sigma-Aldrich; Figs. 3 b and 4 c). When the latter antibody was used, isotype-specific secondary antibodies directed against the antiacetylated tubulin (anti–mouse IgG2b Alexa Fluor 488; Invitrogen) and antitubulin (anti–mouse IgG1 Alexa Fluor 647; Invitrogen) primary antibodies were used for detection.

Immunofluorescence microscopy

For the images in Figs. 2 (j–l) and 4 b, fluorescence was viewed with a DMRXA microscope using a plan apochromat 100×, 1.4 numerical aperture oil immersion objective with a 1.6× optivar (1 pixel = 0.039 µm) and a filter set (Chroma 71001A; Chroma Technology Corp.). 1- or 2-s exposures were captured using a Retiga EX-cooled CCD camera driven by MetaMorph v.6.1.2 software. To produce the final image, the summed maxima of up to 10 images from a Z series (captured at 0.5-µm intervals) for each wavelength were colored (red for Alexa Fluor 594, green or blue for Alexa Fluor 488, and blue for Alexa Fluor 647), merged and adjusted for brightness in ImageJ software (National Institutes of Health), and cropped and sized in Photoshop (Adobe Systems Inc.).

For the remainder of the images, fluorescence was viewed using a live cell imaging system (Deltavison RT; Applied Precision) with a 100×, 1.4 numerical aperture objective (Olympus) with a 1.6× optivar and appropriate filter sets. Images were captured with a camera (CoolSnap HQ CCD; Photometrics). Postacquisition deconvolution was performed using SoftWorx software (Applied Precision). The final images were produced as described for Figs. 2 (j–l) and 4 b in this section.

Data analysis

Distances R1 (from the basal bodies to the posterior end of the longest aceylated rootlet), R2 (from the basal bodies to the posterior end of the second longest aceylated rootlet), and L (cell length) in wild-type and *mlt1* cells were obtained from the summed Z series for Alexa Fluor 488 (specific for antiacetylated tubulin) using the MetaMorph measure distance tool. Distances E1 (from the basal bodies to the posterior edge of ChR1 patch fluorescence), E2 (from the basal bodies to the posterior edge of the second most posterior ChR1 patch), and L (cell length) in wild-type, *mlt1*, or *mlt1 uni1* cells were obtained using the SoftWorx measure tool. The distance measurements were transferred to a spreadsheet (Excel; Microsoft), which was used to obtain the mean and SD values presented in Table I and in the text. Excel was also used to determine the p-value (at $\alpha = 0.05$) reflecting the statistical significance of differences between the measurements obtained from wild-type versus *mlt1* or *mlt1 uni1* cells using the two-sample (assuming unequal variances) *t* test (Table I).

For Fig. 7 e, the SoftWorx data inspector tool was used to determine the mean pixel value within a 15 × 15–pixel square surrounding an anterior "spot" of ChR1-specific Alexa Fluor 594 fluorescence in wild-type (flagellate) or mutant (aflagellate) cells that had been mixed before immunolabeling. A mean background pixel intensity (mean value of 15 × 15–pixel squares measured from elsewhere in the cell body of each cell) was subtracted from each anterior spot value, and mean and SD values were obtained in Excel as described in this section. Using the two-sample (assuming unequal variances) *t* test, the values obtained from wild-type cells ($n = 66$) differed significantly from those obtained from either *fla8-1* cells ($n = 64$) or *fla15-1* ($n = 43$) cells (P (0.05) = 2.35×10^{-7} and 3.78×10^{-5}, respectively).

Figures

Figures were produced using Illustrator (Adobe Systems Inc.) to combine the final images (imported as TIF files from Photoshop) with text and diagrams. The graph in Fig. 7 e was produced in Excel and copied to the Illustrator file.

Online supplemental material

Fig. S1 shows bright field micrographs of aberrant eyespots in *asq2*, *vfl2*, and *bld2* mutant cells; images were obtained as described in the Light microscopy section. Online supplemental material is available at http://www.jcb.org/cgi/content/full/jcb.201009131/DC1.

The authors would like to thank Peter Hegemann for the gift of the polyclonal anti-ChR1 serum, Wallace Marshall for the *asq2-1* mutant strain, and Elizabeth Harris and Matt Laudon of the *Chlamydomonas* Resource Center for the reliable supply of several mutant strains. We also thank Carl Boswell and members of the Parker laboratory at the University of Arizona for assistance with microscopy, Karl-Ferdinand Lechtreck (University of Massachusetts Medical School, Worcester, MA) for suggesting the use of isotype-specific secondary antibodies, and Frans Tax, Kim McDermott, Bill Saxton, Kathy Osteryoung, and Alison Adams for helpful suggestions concerning the manuscript.

This work was supported by National Science Foundation grant MCB-0843094 to C.L. Dieckmann.

Submitted: 27 September 2010
Accepted: 6 April 2011

References

Abrash, E.B., and D.C. Bergmann. 2009. Asymmetric cell divisions: a view from plant development. *Dev. Cell*. 16:783–796. doi:10.1016/j.devcel.2009.05.014

Anderson, C.T., and T. Stearns. 2009. Centriole age underlies asynchronous primary cilium growth in mammalian cells. *Curr. Biol.* 19:1498–1502. doi:10.1016/j.cub.2009.07.034

Baldari, C.T., and J. Rosenbaum. 2010. Intraflagellar transport: it's not just for cilia anymore. *Curr. Opin. Cell Biol.* 22:75–80. doi:10.1016/j.ceb.2009.10.010

Berthold, P., S.P. Tsunoda, O.P. Ernst, W. Mages, D. Gradmann, and P. Hegemann. 2008. Channelrhodopsin-1 initiates phototaxis and photophobic responses in *Chlamydomonas* by immediate light-induced depolarization. *Plant Cell*. 20:1665–1677. doi:10.1105/tpc.108.057919

Boyd, J.S., T.M. Mittelmeier, M.R. Lamb, and C.L. Dieckmann. 2011. Thioredoxin-family protein EYE2 and Ser/Thr kinase EYE3 play interdependent roles in eyespot assembly. *Mol Biol Cell*. doi:10.1091 /mbc.E10-11-0918.

Brazelton, W.J., C.D. Amundsen, C.D. Silflow, and P.A. Lefebvre. 2001. The *bld1* mutation identifies the *Chlamydomonas* osm-6 homolog as a gene required for flagellar assembly. *Curr. Biol.* 11:1591–1594. doi:10.1016/S0960-9822(01)00485-7

Coquelle, F.M., B. Vitre, and I. Arnal. 2009. Structural basis of EB1 effects on microtubule dynamics. *Biochem. Soc. Trans.* 37:997–1001. doi:10.1042/BST0370997

Deane, J.A., D.G. Cole, E.S. Seeley, D.R. Diener, and J.L. Rosenbaum. 2001. Localization of intraflagellar transport protein IFT52 identifies basal body transitional fibers as the docking site for IFT particles. *Curr. Biol.* 11:1586–1590. doi:10.1016/S0960-9822(01)00484-5

Dieckmann, C.L. 2003. Eyespot placement and assembly in the green alga *Chlamydomonas*. *Bioessays*. 25:410–416. doi:10.1002/bies.10259

Dutcher, S.K. 2003. Elucidation of basal body and centriole functions in *Chlamydomonas reinhardtii*. *Traffic*. 4:443–451. doi:10.1034/j.1600-0854.2003.00104.x

Dutcher, S.K., and E.C. Trabuco. 1998. The *UNI3* gene is required for assembly of basal bodies of *Chlamydomonas* and encodes delta-tubulin, a new member of the tubulin superfamily. *Mol. Biol. Cell*. 9:1293–1308.

Dutcher, S.K., N.S. Morrissette, A.M. Preble, C. Rackley, and J. Stanga. 2002. Epsilon-tubulin is an essential component of the centriole. *Mol. Biol. Cell*. 13:3859–3869. doi:10.1091/mbc.E02-04-0205

Ehler, L.L., and S.K. Dutcher. 1998. Pharmacological and genetic evidence for a role of rootlet and phycoplast microtubules in the positioning and assembly of cleavage furrows in *Chlamydomonas reinhardtii*. *Cell Motil. Cytoskeleton*. 40:193–207. doi:10.1002/(SICI)1097-0169(1998)40:2<193::AID-CM8>3.0.CO;2-G

Ehler, L.L., J.A. Holmes, and S.K. Dutcher. 1995. Loss of spatial control of the mitotic spindle apparatus in a *Chlamydomonas reinhardtii* mutant strain lacking basal bodies. *Genetics*. 141:945–960.

Ermilova, E.V., Z.M. Zalutskaya, and B.V. Gromov. 1993. Chemotaxis towards sugars in *Chlamydomonas reinhardtii*. *Curr. Microbiol.* 27:47–50. doi:10.1007/BF01576833

Feldman, J.L., and W.F. Marshall. 2009. *ASQ2* encodes a TBCC-like protein required for mother-daughter centriole linkage and mitotic spindle orientation. *Curr. Biol.* 19:1238–1243. doi:10.1016/j.cub.2009.05.071

Feldman, J.L., S. Geimer, and W.F. Marshall. 2007. The mother centriole plays an instructive role in defining cell geometry. *PLoS Biol.* 5:e149. doi:10.1371/journal.pbio.0050149

Foster, K.W., and R.D. Smyth. 1980. Light Antennas in phototactic algae. *Microbiol. Rev.* 44:572–630.

Geimer, S., and M. Melkonian. 2004. The ultrastructure of the *Chlamydomonas reinhardtii* basal apparatus: identification of an early marker of radial asymmetry inherent in the basal body. *J. Cell Sci.* 117:2663–2674. doi:10.1242/jcs.01120

Geimer, S., and M. Melkonian. 2005. Centrin scaffold in *Chlamydomonas reinhardtii* revealed by immunoelectron microscopy. *Eukaryot. Cell*. 4:1253–1263. doi:10.1128/EC.4.7.1253-1263.2005

Gönczy, P. 2008. Mechanisms of asymmetric cell division: flies and worms pave the way. *Nat. Rev. Mol. Cell Biol.* 9:355–366. doi:10.1038/nrm2388

Goodenough, U.W., and H.S. StClair. 1975. BALD-2: a mutation affecting the formation of doublet and triplet sets of microtubules in *Chlamydomonas reinhardtii*. *J. Cell Biol.* 66:480–491. doi:10.1083/jcb.66.3.480

Govorunova, E.G., K.H. Jung, O.A. Sineshchekov, and J.L. Spudich. 2004. *Chlamydomonas* sensory rhodopsins A and B: cellular content and role in photophobic responses. *Biophys. J.* 86:2342–2349. doi:10.1016/S0006-3495(04)74291-5

Gruber, H.E., and B. Rosario. 1974. Variation in eyespot ultrastructure in *Chlamydomonas reinhardi* (ac-31). *J. Cell Sci.* 15:481–494.

Hammond, J.W., D.W. Cai, and K.J. Verhey. 2008. Tubulin modifications and their cellular functions. *Curr. Opin. Cell Biol.* 20:71–76. doi:10.1016/j.ceb.2007.11.010

Harris, E.H. 2001. *Chlamydomonas* as a model organism. *Annu. Rev. Plant Physiol. Plant Mol. Biol.* 52:363–406. doi:10.1146/annurev.arplant.52.1.363

Harris, E. 2009. The *Chlamydomonas* Sourcebook. Vol. 1–3. Second edition. D. Stern and G. Witman, editors. Academic Press, San Diego, CA. 2,000 pp.

Holmes, J.A., and S.K. Dutcher. 1989. Cellular asymmetry in *Chlamydomonas reinhardtii. J. Cell Sci.* 94:273–285.

Huang, B., Z. Ramanis, S.K. Dutcher, and D.J. Luck. 1982. Uniflagellar mutants of *Chlamydomonas*: evidence for the role of basal bodies in transmission of positional information. *Cell*. 29:745–753. doi:10.1016/0092-8674(82)90436-6

Iomini, C., V. Babaev-Khaimov, M. Sassaroli, and G. Piperno. 2001. Protein particles in *Chlamydomonas* flagella undergo a transport cycle consisting of four phases. *J. Cell Biol.* 153:13–24. doi:10.1083/jcb.153.1.13

Iomini, C., J.E. Till, and S.K. Dutcher. 2009. Genetic and phenotypic analysis of flagellar assembly mutants in *Chlamydomonas reinhardtii. Methods Cell Biol.* 93:121–143. doi:10.1016/S0091-679X(08)93007-7

Johnson, U.G., and K.R. Porter. 1968. Fine structure of cell division in *Chlamydomonas reinhardi*. Basal bodies and microtubules. *J. Cell Biol.* 38:403–425. doi:10.1083/jcb.38.2.403

Kamiya, R., and E. Hasegawa. 1987. Intrinsic difference in beat frequency between the two flagella of *Chlamydomonas reinhardtii*. *Exp. Cell Res.* 173:299–304. doi:10.1016/0014-4827(87)90357-0

Kamiya, R., and G.B. Witman. 1984. Submicromolar levels of calcium control the balance of beating between the two flagella in demembranated models of *Chlamydomonas. J. Cell Biol.* 98:97–107. doi:10.1083/jcb.98.1.97

Kateriya, S., G. Nagel, E. Bamberg, and P. Hegemann. 2004. "Vision" in single-celled algae. *News Physiol. Sci.* 19:133–137.

Koblenz, B., J. Schoppmeier, A. Grunow, and K.F. Lechtreck. 2003. Centrin deficiency in *Chlamydomonas* causes defects in basal body replication, segregation and maturation. *J. Cell Sci.* 116:2635–2646. doi:10.1242/jcs.00497

Kreimer, G. 2009. The green algal eyespot apparatus: a primordial visual system and more? *Curr. Genet.* 55:19–43. doi:10.1007/s00294-008-0224-8

Lamb, M.R., S.K. Dutcher, C.K. Worley, and C.L. Dieckmann. 1999. Eyespot-assembly mutants in *Chlamydomonas reinhardtii. Genetics*. 153:721–729.

Lawson, M.A., and P. Satir. 1994. Characterization of the eyespot regions of "blind" *Chlamydomonas* mutants after restoration of photophobic responses. *J. Eukaryot. Microbiol.* 41:593–601. doi:10.1111/j.1550-7408.1994.tb01521.x

Lechtreck, K.F., and M. Melkonian. 1991. Striated microtubule-associated fibers: identification of assemblin, a novel 34-kD protein that forms paracrystals of 2-nm filaments in vitro. *J. Cell Biol.* 115:705–716. doi:10.1083/jcb.115.3.705

Lechtreck, K.F., and C.D. Silflow. 1997. SF-assemblin in *Chlamydomonas*: sequence conservation and localization during the cell cycle. *Cell Motil. Cytoskeleton*. 36:190–201. doi:10.1002/(SICI)1097-0169(1997)36:2<190::AID-CM8>3.0.CO;2-D

LeDizet, M., and G. Piperno. 1986. Cytoplasmic microtubules containing acetylated α-tubulin in *Chlamydomonas reinhardtii*: spatial arrangement and properties. *J. Cell Biol.* 103:13–22. doi:10.1083/jcb.103.1.13

Li, R., and G.G. Gundersen. 2008. Beyond polymer polarity: how the cytoskeleton builds a polarized cell. *Nat. Rev. Mol. Cell Biol.* 9:860–873. doi:10.1038/nrm2522

Melkonian, M., and H. Robenek. 1980. Eyespot membranes of *Chlamydomonas reinhardii*: a freeze-fracture study. *J. Ultrastruct. Res.* 72:90–102. doi:10.1016/S0022-5320(80)90138-0

Merchant, S.S., S.E. Prochnik, O. Vallon, E.H. Harris, S.J. Karpowicz, G.B. Witman, A. Terry, A. Salamov, L.K. Fritz-Laylin, L. Maréchal-Drouard, et al. 2007. The *Chlamydomonas* genome reveals the evolution of key animal and plant functions. *Science*. 318:245–250. doi:10.1126/science.1143609

Miller, M.S., J.M. Esparza, A.M. Lippa, F.G. Lux III, D.G. Cole, and S.K. Dutcher. 2005. Mutant kinesin-2 motor subunits increase chromosome loss. *Mol. Biol. Cell*. 16:3810–3820. doi:10.1091/mbc. E05-05-0404

Mittelmeier, T.M., P. Berthold, A. Danon, M.R. Lamb, A. Levitan, M.E. Rice, and C.L. Dieckmann. 2008. C2 domain protein MIN1 promotes eyespot organization in *Chlamydomonas reinhardtii. Eukaryot. Cell*. 7:2100–2112. doi:10.1128/EC.00118-08

Moestrup, Ø. 1978. On the phylogenetic validity of the flagellar apparatus in green algae and other chlorophyll A and B containing plants. *Biosystems*. 10:117–144. doi:10.1016/0303-2647(78)90035-7

Mueller, J., C.A. Perrone, R. Bower, D.G. Cole, and M.E. Porter. 2005. The FLA3 KAP subunit is required for localization of kinesin-2 to the site of flagellar assembly and processive anterograde intraflagellar transport. *Mol. Biol. Cell*. 16:1341–1354. doi:10.1091/mbc.E04-10-0931

Nagel, G., D. Ollig, M. Fuhrmann, S. Kateriya, A.M. Musti, E. Bamberg, and P. Hegemann. 2002. Channelrhodopsin-1: a light-gated proton channel in green algae. *Science*. 296:2395–2398. doi:10.1126/science.1072068

Pazour, G.J., B.L. Dickert, and G.B. Witman. 1999. The DHC1b (DHC2) isoform of cytoplasmic dynein is required for flagellar assembly. *J. Cell Biol.* 144:473–481. doi:10.1083/jcb.144.3.473

Peters, N.T., and D.L. Kropf. 2010. Asymmetric microtubule arrays organize the endoplasmic reticulum during polarity establishment in the brown alga *Silvetia compressa. Cytoskeleton (Hoboken)*. 67:102–111. doi:10.1002/cm.20427

Piasecki, B.P., and C.D. Silflow. 2009. The *UNI1* and *UNI2* genes function in the transition of triplet to doublet microtubules between the centriole and cilium in *Chlamydomonas. Mol. Biol. Cell*. 20:368–378. doi:10.1091/mbc.E08-09-0900

Piasecki, B.P., M. LaVoie, L.W. Tam, P.A. Lefebvre, and C.D. Silflow. 2008. The Uni2 phosphoprotein is a cell cycle regulated component of the basal body maturation pathway in *Chlamydomonas reinhardtii. Mol. Biol. Cell*. 19:262–273. doi:10.1091/mbc.E07-08-0798

Piel, M., P. Meyer, A. Khodjakov, C.L. Rieder, and M. Bornens. 2000. The respective contributions of the mother and daughter centrioles to centrosome activity and behavior in vertebrate cells. *J. Cell Biol.* 149:317–330. doi:10.1083/jcb.149.2.317

Piperno, G., and M.T. Fuller. 1985. Monoclonal antibodies specific for an acetylated form of α-tubulin recognize the antigen in cilia and flagella from a variety of organisms. *J. Cell Biol.* 101:2085–2094. doi:10.1083/jcb.101.6.2085

Piperno, G., E. Siuda, S. Henderson, M. Segil, H. Vaananen, and M. Sassaroli. 1998. Distinct mutants of retrograde intraflagellar transport (IFT) share similar morphological and molecular defects. *J. Cell Biol.* 143:1591–1601. doi:10.1083/jcb.143.6.1591

Porter, M.E., R. Bower, J.A. Knott, P. Byrd, and W. Dentler. 1999. Cytoplasmic dynein heavy chain 1b is required for flagellar assembly in *Chlamydomonas. Mol. Biol. Cell*. 10:693–712.

Poulain, F.E., and A. Sobel. 2010. The microtubule network and neuronal morphogenesis: dynamic and coordinated orchestration through multiple players. *Mol. Cell. Neurosci.* 43:15–32. doi:10.1016/j.mcn.2009.07.012

Qin, H.M., Z.H. Wang, D. Diener, and J. Rosenbaum. 2007. Intraflagellar transport protein 27 is a small G protein involved in cell-cycle control. *Curr. Biol.* 17:193–202. doi:10.1016/j.cub.2006.12.040

Quinn, C.C., and W.G. Wadsworth. 2008. Axon guidance: asymmetric signaling orients polarized outgrowth. *Trends Cell Biol.* 18:597–603. doi:10.1016/j.tcb.2008.09.005

Richardson, D.N., M.P. Simmons, and A.S.N. Reddy. 2006. Comprehensive comparative analysis of kinesins in photosynthetic eukaryotes. *BMC Genomics*. 7:18. doi:10.1186/1471-2164-7-18

Ringo, D.L. 1967. Flagellar motion and fine structure of the flagellar apparatus in *Chlamydomonas*. *J. Cell Biol.* 33:543–571. doi:10.1083/jcb.33.3.543

Riparbelli, M.G., R. Dallai, D. Mercati, Y. Bu, and G. Callaini. 2009. Centriole symmetry: a big tale from small organisms. *Cell Motil. Cytoskeleton*. 66:1100–1105. doi:10.1002/cm.20417

Roberts, A.M. 2006. Mechanisms of gravitaxis in *Chlamydomonas. Biol. Bull.* 210:78–80. doi:10.2307/4134597

Roberts, D.G.W., M.R. Lamb, and C.L. Dieckmann. 2001. Characterization of the *EYE2* gene required for eyespot assembly in *Chlamydomonas reinhardtii. Genetics*. 158:1037–1049.

Rüffer, U., and W. Nultsch. 1991. Flagellar photoresponses of *Chlamydomonas* cells held on micropipettes: II. Change in flagellar beat pattern. *Cell Motil. Cytoskeleton*. 18:269–278. doi:10.1002/cm.970180404

Rüffer, U., and W. Nultsch. 1998. Flagellar coordination in *Chlamydomonas* cells held on micropipettes. *Cell Motil. Cytoskeleton*. 41:297–307. doi:10.1002/(SICI)1097-0169(1998)41:4<297::AID-CM3>3.0.CO;2-Y

Sann, S., Z.P. Wang, H. Brown, and Y.S. Jin. 2009. Roles of endosomal trafficking in neurite outgrowth and guidance. *Trends Cell Biol.* 19:317–324. doi:10.1016/j.tcb.2009.05.001

Sawa, H. 2010. Specification of neurons through asymmetric cell divisions. *Curr. Opin. Neurobiol.* 20:44–49. doi:10.1016/j.conb.2009.09.014

Sjoblad, R.D., and P.H. Frederikse. 1981. Chemotactic responses of *Chlamydomonas reinhardtii*. *Mol. Cell. Biol.* 1:1057–1060.

St Johnston, D., and J. Ahringer. 2010. Cell polarity in eggs and epithelia: parallels and diversity. *Cell*. 141:757–774. doi:10.1016/j.cell.2010.05.011

Suzuki, T., K. Yamasaki, S. Fujita, K. Oda, M. Iseki, K. Yoshida, M. Watanabe, H. Daiyasu, H. Toh, E. Asamizu, et al. 2003. Archaeal-type rhodopsins in *Chlamydomonas*: model structure and intracellular localization. *Biochem. Biophys. Res. Commun.* 301:711–717. doi:10.1016/S0006-291X(02)03079-6

Taillon, B.E., S.A. Adler, J.P. Suhan, and J.W. Jarvik. 1992. Mutational analysis of centrin: an EF-hand protein associated with three distinct contractile fibers in the basal body apparatus of *Chlamydomonas*. *J. Cell Biol.* 119:1613–1624. doi:10.1083/jcb.119.6.1613

Takada, S., and R. Kamiya. 1997. Beat frequency difference between the two flagella of *Chlamydomonas* depends on the attachment site of outer dynein arms on the outer-doublet microtubules. *Cell Motil. Cytoskeleton*. 36:68–75. doi:10.1002/(SICI)1097-0169(1997)36:1<68::AID-CM6>3.0.CO;2-D

Vashishtha, M., Z. Walther, and J.L. Hall. 1996. The kinesin-homologous protein encoded by the *Chlamydomonas FLA10* gene is associated with basal bodies and centrioles. *J. Cell Sci.* 109:541–549.

Vinogradova, T., P.M. Miller, and I. Kaverina. 2009. Microtubule network asymmetry in motile cells: role of Golgi-derived array. *Cell Cycle*. 8:2168–2174. doi:10.4161/cc.8.14.9074

Walther, Z., M. Vashishtha, and J.L. Hall. 1994. The *Chlamydomonas FLA10* gene encodes a novel kinesin-homologous protein. *J. Cell Biol.* 126:175–188. doi:10.1083/jcb.126.1.175

Wang, X.Q., J.W. Tsai, J.H. Imai, W.N. Lian, R.B. Vallee, and S.H. Shi. 2009. Asymmetric centrosome inheritance maintains neural progenitors in the neocortex. *Nature*. 461:947–955. doi:10.1038/nature08435

Witman, G.B. 1993. *Chlamydomonas* phototaxis. *Trends Cell Biol.* 3:403–408. doi:10.1016/0962-8924(93)90091-E

Wright, R.L., J. Salisbury, and J.W. Jarvik. 1985. A nucleus-basal body connector in *Chlamydomonas* reinhardtii that may function in basal body localization or segregation. *J. Cell Biol.* 101:1903–1912. doi:10.1083/jcb.101.5.1903

Wright, R.L., S.A. Adler, J.G. Spanier, and J.W. Jarvik. 1989. Nucleus-basal body connector in *Chlamydomonas*: evidence for a role in basal body segregation and against essential roles in mitosis or in determining cell polarity. *Cell Motil. Cytoskeleton*. 14:516–526. doi:10.1002/cm.970140409

Yamashita, Y.M. 2009. The centrosome and asymmetric cell division. *Prion*. 3:84–88. doi:10.4161/pri.3.2.8821

Yoshimura, K., Y. Matsuo, and R. Kamiya. 2003. Gravitaxis in *Chlamydomonas reinhardtii* studied with novel mutants. *Plant Cell Physiol.* 44:1112–1118. doi:10.1093/pcp/pcg134